The recombination landscape in wild house mice inferred using population genomic data

Tom R. Booker[1], Rob W. Ness[2], Peter D. Keightley[1]

[1]*Institute of Evolutionary Biology, University of Edinburgh, Edinburgh, EH9 3FL, United Kingdom*

[2]*Department of Biology, University of Toronto Mississauga, Mississauga, ON, Canada*

Abstract

Characterizing variation in the rate of recombination across the genome is important for understanding many evolutionary processes. The landscape of recombination has been studied previously in the house mouse, *Mus musculus*, and it is known that the different subspecies exhibit different suites of recombination hotspots. However, it is not established whether broad-scale variation in the rate of recombination is conserved between the subspecies. In this study, we construct a fine-scale recombination map for the Eastern house mouse subspecies, *M. m. castaneus*, using 10 individuals sampled from its ancestral range. After inferring phase, we use LDhelmet to construct recombination maps for each autosome. We find that the spatial distribution of recombination rate is strongly positively between our *castaneus* map and a map constructed using inbred lines of mice derived predominantly from *M. m. domesticus*. We also find that levels of genetic diversity in *M. m. castaneus* are positively correlated with the rate of recombination, consistent with pervasive natural selection acting in the genome. Our study suggests that recombination rate variation is conserved at broad scales between *M. musculus* subspecies.

Introduction

In many species, rates of crossing-over are not uniformly distributed across chromosomes, and understanding this variation and its causes is important for many aspects of molecular evolution. Experiments in laboratory strains or managed populations examining the inheritance of markers through pedigrees have allowed direct estimation of rates of crossing over in different regions of the genome. Studies of this kind are impractical for many wild populations, where pedigree structures are largely unknown (but see Johnston *et al.* 2016). In mice, there have been multiple genetic maps published (e.g. Jensen-Seaman *et al.* 2004; Paigen *et al.* 2008; Cox *et al.* 2009; Liu *et al.* 2014), typically using the classical inbred laboratory strains, which are predominantly derived from the Western European house mouse subspecies, *Mus musculus domesticus* (Yang *et al.* 2011). Recombination rate variation in laboratory strains may not, therefore, reflect natural rates and patterns in wild mice of different subspecies. In addition, recombination rate modifiers may have become fixed in the process of laboratory strain management. On the other hand, directly estimating recombination rates in wild house mice is not feasible without both a population's pedigree and many genotyped individuals (but see Wang *et al.* 2017).

To understand variation in recombination rates, patterns of linkage disequilibrium (LD) in a sample of individuals drawn from a population can be used. Coalescent-based methods have been developed that use such data to indirectly estimate recombination rates at very fine scales (Hudson 2001; Mcvean *et al.* 2002; Mcvean *et al.* 2004; Auton and Mcvean 2007; Chan *et al.* 2012). The recombination rates estimated in this way reflect variation in crossing over rates in populations

ancestral to the extant population, and are averages between the sexes. Methods using LD have been applied to explore variation in recombination rates among mammals and other eukaryotes, and have demonstrated that recombination hotspots are associated with specific genomic features (Myers *et al.* 2010; Paigen and Petkov 2010; Singhal *et al.* 2015).

The underlying mechanisms explaining the locations of recombination events have been the focus of much research. In house mice and in most other mammals, the PRDM9 zinc-finger protein binds to specific DNA motifs, resulting in an increased probability of double-strand breaks, which can then be resolved by reciprocal crossing-over (Grey *et al.* 2011; Baudat *et al.* 2013). Accordingly, it has been shown that recombination hotspots are enriched for PRDM9 binding sites (Myers *et al.* 2010; Brunschwig *et al.* 2012). PRDM9-knockout mice still exhibit hotspots, but in dramatically different genomic regions (Brick *et al.* 2012). Variation in PRDM9, specifically in the exon encoding the zinc-finger array, results in different binding motifs (Baudat *et al.* 2010). Davies *et al.* (2016) generated a line of mice in which the exon encoding the portion of the PRDM9 protein specifying the DNA binding motif was replaced with the orthologous human sequence. The recombination hotspots they observed in this ‘humanized’ line of mice were enriched for the PRDM9 binding motif observed in humans.

Great ape species have different alleles of the PRDM9 gene (Schwartz *et al.* 2014) and relatively little hotspot sharing (Winckler *et al.* 2005; Stevison *et al.* 2015). Correlations between the broad-scale recombination landscapes of the great apes are, however, relatively strongly positive (Stevison *et al.* 2011; Stevison *et al.* 2015).

This suggests that, while hotspots evolve rapidly, the overall genetic map changes more slowly. Indeed, multiple closely related species pairs with different hotspot locations show correlations between recombination rates at broad scales (Smukowski and Noor 2011), as do species that share hotspots or lack them altogether (Singhal *et al.* 2015; Smukowski Heil *et al.* 2015).

It has been suggested that a population ancestral to the *M. musculus* species complex began to split into the present day subspecies around 500,000 years ago (Geraldes *et al.* 2008). In this time, functionally distinct alleles of the PRDM9 gene and different suites of hotspots have evolved in the subspecies (Smagulova *et al.* 2016). In addition, between members of the *M. musculus* subspecies complex, there is also variation in recombination rates at relatively broad scales for multiple regions of the genome (Dumont *et al.* 2011), and there is genetic variation in recombination rate is polymorphic between *M. m. domesticus* individuals (Wang *et al.* 2017). Brunschwig *et al.* (2012) analyzed single nucleotide polymorphism (SNP) data for classical laboratory strains of mice, and used an LD-based approach to estimate the sex-averaged recombination landscape for the 19 mouse autosomes. The recombination rate map they constructed is similar to a genetic map generated using crosses by Cox *et al.* (2009). Both studies were conducted using the classical inbred lines (whose ancestry is largely *M. m. domesticus*), and their estimated recombination rate landscapes may therefore reflect that of *M. m. domesticus* more than other members of the *M. musculus* species complex.

In this study, we construct a recombination map for the house mouse subspecies *M. m. castaneus*. We used the genome sequences of 10 wild-caught

126 individuals of *M. m. castaneus* from the species' expected ancestral range, originally
127 reported by Halligan *et al.* (2013). In our analysis, we first phased SNPs and
128 estimated rates of error in phasing. Secondly, we simulated data to assess the
129 power of estimating recombination rates based on 10 individuals and the extent by
130 which phase errors lead to biased estimates of the rate of recombination. Finally,
131 using an LD-based approach, we inferred a sex-averaged map of recombination
132 rates and compared this to previously published genetic maps for *M. musculus*. We
133 show that variation in recombination rates in *M. m. castaneus* is very similar to rate
134 variation estimated in the classical inbred strains. This suggests that, at broad
135 scales, recombination rates have been relatively highly conserved since the
136 subspecies began to diverge.
137
138 **Materials and Methods**
139
140 *Polymorphism data for* Mus musculus castaneus
141
142 We analyzed the genomes of 10 wild-caught *M. m. castaneus* individuals
143 sequenced by Halligan *et al.* (2013). Samples were from North-West India, a region
144 that is believed to be within the ancestral range of the house mouse. Mice from this
145 region have among the highest levels of genetic diversity among the *M. musculus*
146 subspecies (Baines and Harr 2007). In addition, the individuals sequenced represent
147 a single population cluster and showed little evidence for substantial inbreeding
148 (Halligan *et al.* 2010). Halligan *et al.* (2013) sequenced individual genomes to high
149 coverage using multiple libraries of Illumina paired-end reads, which were mapped to
150 the mm9 reference genome using BWA (Li and Durbin 2009). Mean coverage was

>20x and the proportion of the genome with >10x coverage was more than 80% for all individuals sampled (Halligan *et al.* 2013). Variants were called with the Samtools *mpileup* function (Li *et al.* 2009) using an allele frequency spectrum (AFS) prior. The AFS was obtained by iteratively calling variants until the spectrum converged. After the first iteration, all SNPs at frequencies >0.5 were swapped into the mm9 genome to construct a reference genome for *M. m. castaneus,* which was used for subsequent variant calling (for further details see Halligan *et al.* 2013). The variant call format files generated by Halligan *et al.* (2013) were used in this study. In addition, alignments of *Mus famulus* and *Rattus norvegicus* to the mm9 genome, also generated by Halligan *et al.* (2013), were used as outgroups.

For the purposes of estimating recombination rates, variable sites were filtered on the basis of several conditions: Insertion/deletion polymorphisms were excluded, because the method used to phase variants (*see below*) cannot process these sites. We also excluded sites with more than two alleles and those that failed the Samtools Hardy-Weinberg equilibrium test ($p < 0.002$).

Inferring phase and estimating switch error rates

LDhelmet estimates recombination rates from a sample of phased chromosomes or haplotypes drawn from a population. To estimate haplotypes, heterozygous SNPs called in *M. m. castaneus* were phased using read-aware phasing in ShapeIt2 (Delaneau *et al.* 2013). ShapeIt2 uses sequencing reads that span multiple heterozygous variants, phase-informative reads (PIRs), and LD to phase variants at the level of whole chromosomes. Incorrectly phased heterozygous

SNPs, termed switch errors, may upwardly bias estimates of the recombination rate, because they appear identical to legitimate crossing over events. To assess the impact of incorrect phasing on our recombination rate inferences, we quantified the switch error rate as follows. The population sample of *M. m. castaneus* comprised of seven females and three males. The X-chromosome variants in males therefore represent perfectly phased haplotypes. We merged the BAM alignments of short reads for the X-chromosome of the three males (samples H12, H28 and H34 from Halligan *et al.* (2013)) to make three datasets of pseudo-females, which are female-like, but in which the true haplotypes are known (H12+H28 = H40; H12+H34 = H46; H28 + H34 = H62). We then jointly re-called variants in the seven female samples plus the three pseudo-females using an identical pipeline as used by Halligan *et al.* (2013), as outlined above, using the same AFS prior.

Switch error rates in Shapeit2 are sensitive both to coverage and quality (per genotype and per variant) (Delaneau *et al.* 2013). We explored the effects of different filter parameters on the switch error rates produced by ShapeIt2 using the X-chromosomes of the pseudo-females. We filtered SNPs based on combinations of variant and genotype quality scores (QUAL and GQ, respectively) and on an individual's sequencing depth (DP) (Table S1). For the individual-specific statistics (DP and GQ), if a single individual failed a particular filter, then that SNP was not included in further analyses. By comparing the known X-chromosome haplotypes and those inferred by ShapeIt2, we calculated switch error rates as the ratio of incorrectly resolved heterozygous SNPs to the total number of heterozygous SNPs for each pseudo-female individual. We used these results to choose filter parameters to apply to the autosomal data that generated a low switch error rate in ShapeIt2,

while maintaining a high number of heterozygous SNPs. We obtained 20 phased haplotypes for each of the 19 mouse autosomes. With these, we estimated the recombination rate landscape for *M. m. castaneus*.

Estimating recombination maps and validation of the approach

LDhelmet (v1.7;Chan *et al.* 2012) generates a sex-averaged map of recombination rates from a sample of haplotypes that are assumed to be drawn from a randomly mating population. Briefly, LDhelmet examines patterns of LD in a sample of phased chromosomal regions and uses a composite likelihood approach to infer recombination rates that are best supported between adjacent SNPs. LDhelmet appears to perform well for species with large effective population size (N_e) and has been shown to be robust to the effects of selective sweeps, which may be prevalent and reduce diversity in and around functional elements of the *M. m. castaneus* genome (Halligan *et al.* 2013). However, the analyses conducted by Chan *et al.* (2012), in which the software was tested, were performed with a larger number of haplotypes than we have in our sample. To assess whether our smaller sample size gives reliable recombination maps, we validated and parameterized LDhelmet using simulated datasets.

A key parameter in LDhelmet is the block penalty, which determines the extent by which likelihood is penalized by spatial variation in the recombination rate, such that a high block penalty results in a smoother recombination map. We performed simulations to determine the block penalty that leads to the most accurate estimates of the recombination rate in chromosomes that have levels of diversity and

base content similar to *M. m. castaneus*. Chromosomes with constant values of ρ ($4N_e r$) ranging from 2×10^{-6} to 2×10^{1} were simulated in SLiM v1.8 (Messer 2013). For each value of ρ, 0.5Mbp of neutrally evolving sequence was simulated for populations of N = 1,000 diploid individuals. Mutation rates in the simulations were set using the compound parameter $\theta = 4N_e\mu$, where μ is the per-base, per-generation mutation rate. The mutation and recombination rates of the simulations were scaled to $\theta/4N$ and $\rho/4N$, respectively. θ was set to 0.01 for all simulations, as this is close to the genome-wide average for our data, based on pairwise differences. Simulations were run for 10,000 generations to achieve equilibrium levels of polymorphism, at which time 10 diploid individuals were sampled from the population. Each simulation was repeated 20 times, resulting in 10Mbp of sequence for each value of ρ. The SLiM output files were converted to sequence data, suitable for analysis by LDhelmet, using a custom Python script that incorporated the mutation rate matrix estimated for non-CpG prone sites in *M. m. castaneus* (see below). We inferred recombination rates from the simulated data in windows of 4,400 SNPs with a 200 SNP overlap between windows, following (Chan *et al.* 2012). We analyzed the simulated data using LDhelmet with block penalties of 10, 25, 50 and 100. The default parameters of LDhelmet are tuned to analyze *Drosophila melanogaster* data (Chan *et al.* 2012). Since the *D. melanogaster* population studied by Chan *et al.* (2012) has comparable levels of genetic diversity to *M. m. castaneus* we used the defaults for all other parameters, other than the block penalty and estimate of θ.

Errors in phase inference, discussed above, may bias our estimates of the recombination rate, since they appear to break apart patterns of LD. We assessed

the impact of these errors on recombination rate inference by incorporating them into the simulated data at a rate estimated from the pseudo-female individuals. For each of the 10 individuals drawn from the simulated populations, switch errors were randomly introduced at heterozygous positions at the rate estimated using the chosen SNP filter set (*see Results*). We then inferred the recombination rates, as above, for the simulated population using these error-prone data. We assessed the effect of switch errors on recombination rate inference by comparing estimates based on the simulated data both with and without switch errors. It is worth noting that there is the potential for switch errors to undo crossing-over events, reducing inferred recombination rates, if they affect heterozygous SNPs that are breakpoints of recombinant regions.

Recombination rate estimation for M. m. castaneus

We used LDhelmet (Chan *et al.* 2012), to estimate recombination rates for each of the *M. m. castaneus* autosomes. It is well established that autosomal recombination rates differ between the sexes in *M musculus* (Cox *et al.* 2009; Liu *et al.* 2014). A drawback of LD-based approaches is that they give sex-averaged recombination rates.

We used both *M. famulus* and *R. norvegicus* as outgroups to assign ancestral alleles to polymorphic sites. LDhelmet incorporates both the mutation matrix and a prior probability on the ancestral allele at each variable position as parameters in the model. We obtained these parameters as follows. For non-CpG prone polymorphic sites, if the outgroups shared the same allele, we assigned that allele as ancestral

and these sites were then used to populate the mutation matrix, following Chan *et al.* (2012). This approach ignores the possibility of both back mutation and homoplasy. To account for this uncertainty, LDhelmet incorporates a prior probability on the ancestral base. Following Singhal *et al.* (2015), at resolvable sites (i.e. when both outgroups agreed), the ancestral base was given a prior probability of 0.91, with 0.03 assigned to each of the three remaining bases. This was done to provide high confidence in the ancestral allele, but to also include the possibility of ancestral allele misinference. At unresolved sites (i.e., if the outgroup alleles did not agree or there were alignment gaps in either outgroup), we used the stationary distribution of allele frequencies from the mutation rate matrix as the prior (Table S2).

We analyzed a total of 43,366,235 SNPs in LDhelmet to construct recombination maps for each of the *M. m. castaneus* autosomes. Following Chan *et al.* (2012), windows of 4,400 SNPs, overlapping by 200 SNPs on either side, were analysed. We ran LDhelmet with a block penalty of 100 for a total of 1,000,000 iterations, discarding the first 100,000 as burn-in. The block penalty value was chosen to obtain a conservatively estimated recombination map, on the basis of the simulation analysis. We analyzed all sites that passed the filters chosen using the pseudo-female phasing regardless of CpG status; note that excluding CpG-prone sites removes ~50% of the available data and thus would substantially reduce the power to infer recombination rates. We assumed $\theta = 0.01$, the approximate genome-wide level of neutral diversity in *M. m. castaneus*, and included ancestral allele priors and the mutation rate matrix for non-CpG sites as parameters in the model. Following the analyses, we removed overlapping SNPs and concatenated SNP windows to obtain recombination maps for whole chromosomes.

It is worthwhile noting that our map was constructed with genotype calls made using the mm9 version of the mouse reference genome. This version was released in 2007 and there have been subsequent versions released since then. However, previously published genetic maps for *M. musculus* were constructed using mm9, so we used that reference to make comparisons (see below).

Comparison to previously published maps

The recombination rate map inferred for *M. m. castaneus* was compared with two previously published genetic maps for *M. musculus*. The first map was generated by analyzing the inheritance patterns of markers in crosses between inbred lines (Cox *et al.* 2009)(downloaded from http://cgd.jax.org/mousemapconverter/). Hereafter, this map shall be referred to as the Cox map. The second map was generated by Brunschwig *et al.* (2012), by analyzing SNPs in a large number of inbred mouse lines using LDhat (Auton and Mcvean 2007), the software upon which LDhelmet is based (available at http://www.genetics.org/content/early/2012/05/04/genetics.112.141036). Hereafter, this map shall be referred to as the Brunschwig map. Both maps were generated using classical strains of laboratory mice, which are predominantly of *M. m. domesticus* origin (Yang *et al.* 2011). Both the Brunschwig and Cox maps were constructed using far fewer markers than the present study, ~250,000 and ~10,000 SNPs, respectively.

325 Recombination rates in the Brunschwig map and our *castaneus* map were
326 inferred in terms of the population recombination rate ($\rho = 4N_e r$), units that are not
327 directly convertible to centimorgans (cM), but were converted to cM/Mb for
328 comparison purposes using frequency weighted means, as follows. Both LDhat and
329 LDhelmet give estimates of ρ (per Kbp and bp, respectively) between pairs of
330 adjacent SNPs. To account for differences in the physical distance between adjacent
331 SNPs when calculating cumulative ρ, we used the number of bases between a pair
332 of SNPs to weight that pair's contribution to the sum. By setting the total map
333 distance for each chromosome to be equal to those found by Cox *et al.* (2009), we
334 scaled the cumulative ρ at each analyzed SNP position to cM values.
335
336 At the level of whole chromosomes, we compared mean recombination rates
337 from the *castaneus* map with several previously published maps. The frequency-
338 weighted mean recombination rates (in terms of ρ) for each of the autosomes from
339 the *castaneus* and Brunschwig maps were compared with the cM/Mb values
340 obtained by Cox *et al.* (2009) as well as independent estimates of the per
341 chromosome recombination rates from Jensen-Seaman *et al.* (2004). Pearson
342 correlations were calculated for each comparison. Population structure in the inbred
343 line data analyzed by Brunschwig *et al.* (2012) may have elevated LD, thus
344 downwardly biasing estimates of ρ. To investigate this, we divided the frequency-
345 weighted mean recombination rates per chromosome from the *castaneus* and
346 Brunschwig maps by the rates given in Cox *et al.* (2009) to obtain estimates of
347 effective population size.
348

At a finer scale, we compared variation in recombination rates across the autosomes in the different maps using windows. We calculated Pearson correlations between the frequency weighted-mean recombination rates (in cM/Mb) in non-overlapping windows for the *castaneus,* Cox and Brunschwig maps. The window size considered may affect the correlation between maps, so we calculate Pearson correlations in windows of 1Mbp to 20Mbp in size. For visual comparison of the *castaneus* and Cox maps, we plotted recombination rates in sliding windows of 10Mbp, offset by 1Mb.

Examining the correlation between nucleotide diversity and recombination rate

There is evidence that natural selection is pervasive in the protein-coding genes and conserved non-coding elements in the murid genome (Halligan *et al.* 2010; Halligan *et al.* 2011; Halligan *et al.* 2013). Directional selection acting on selected sites within exons may reduce diversity at linked neutral sites through the processes of background selection and/or selective sweeps. These processes have the largest effect in regions of low recombination, and can therefore generate positive correlations between diversity and the recombination rate, as has been observed in multiple species (Cutter and Payseur 2013). We used our *castaneus* map to examine the relationship between nucleotide diversity and recombination rates as follows. We obtained the coordinates of the canonical spliceforms of protein coding genes, orthologous between mouse and rat from Ensembl Biomart (Ensembl Database 67; http://www.ensembl.org/info/website/archives/index.html). We calculated the frequency-weighted mean recombination rate and the GC content for each gene. Using the approximate *castaneus* reference, described above, and the

outgroup alignment, we obtained the locations of 4-fold degenerate synonymous sites. If a site was annotated as 4-fold in all three species considered, it was used for further analysis. We removed poor quality alignments between mouse and rat, exhibiting a spurious excess of diverged sites, where >80% of sites were missing. We also excluded five genes that were diverged at all non-CpG prone 4-fold sites, as it is likely that these also represent incorrect alignments. After filtering, there were a total of 18,171 protein-coding genes for analysis.

We examined the correlation between local recombination rates in protein coding genes with nucleotide diversity and divergence. Variation in the mutation rate across the genome may influence genome-wide analyses of nucleotide polymorphism, so we also examined the correlation between the ratio of nucleotide diversity and divergence from *R. norvegicus* at neutral sites and the rate of recombination. We used non-parametric Kendall rank correlations for all comparisons.

All analyses were conducted using custom Python scripts, except correlation analyses which were conducted using R (R Core Team 2016).

Results

Phasing SNPs and estimating the switch error rate

In order to infer recombination rates from our sample of individuals, we required phased SNPs. Taking advantage of the high sequencing depth of the

399 sample, we phased SNPs using ShapeIt2, an approach that makes use of both LD
400 and sequencing reads to resolve haplotypes. We phased each of the mouse
401 autosomes, giving a total of 43,366,235 SNPs for estimation of recombination rates.
402
403 By constructing pseudo-female individuals, we quantified the switch error rate
404 incurred when inferring phase from our data. After filtering of variants, ShapeIt2
405 achieved low switch error rates for all parameter combinations tested (Table S1). We
406 chose a set of filters (GQ > 15, QUAL > 30) that resulted in a mean switch error rates
407 across the three pseudo-females of 0.46% (Table S1). More stringent filtering
408 resulted in slightly lower mean switch error rates, but also resulted in the removal of
409 many more variants from the dataset (Table S1), thus reducing power to resolve
410 recombination rates in downstream analyses.
411
412 *Simulations to validate LDhelmet for the population sample of* M. m. castaneus
413
414 We assessed the performance of LDhelmet when applied to our dataset by
415 simulation. In the absence of switch errors, LDhelmet accurately infers the average
416 recombination rate down to values of ρ/bp = 2×10^{-4} (Figure 1). Below this value,
417 LDhelmet overestimated the scaled recombination rate for the simulated populations
418 (Figure 1). With switch errors incorporated into simulated data, LDhelmet accurately
419 estimated ρ/bp in the range 2×10^{-3} to 2×10^{2}. When the true ρ/bp was $< 2 \times 10^{-3}$,
420 however, LDhelmet overestimated the mean recombination rate for 0.5Mbp regions
421 (Figure 1). This behavior was consistent for all block penalties tested (Figure S1).
422 Given that the simulations incorporated the mutation rate matrix (Table S2) and
423 mutation rate ($\theta = 4N_e\mu$) estimated for *M. m. castaneus* we concluded that LDhelmet

is applicable to the dataset of 10 *M. m. castaneus* individuals sequenced by Halligan *et al.* (2013).

Recombination rates across the M. m. castaneus *autosomes*

A recombination rate map for each *M. m. castaneus* autosome was constructed using LDhelmet. We analyzed a total of 43,366,235 phased SNPs across the 19 mouse autosomes. The frequency weighted mean value of ρ/bp for all autosomes was 0.009. This value is greater than the lower detection limit suggested by both the simulations with and without switch errors (Figure 1).

We assessed variation in whole-chromosome recombination rates between our LD-based *castaneus* map and direct estimates of recombination rates published in earlier studies. Comparing the mean recombination rates for whole chromosomes provides us with a baseline comparison for which we have an *a priori* expectation: we expect that chromosome 19, the shortest in physical length, should have the highest mean recombination rate, since at least one crossing over event is required per meiosis per chromosome in mice. This has been demonstrated in previous studies of recombination in *M.* musculus (Jensen-Seaman *et al.* 2004; Cox *et al.* 2009). Indeed, we find that the frequency-weighted mean recombination rate for chromosome 19 is the highest among the autosomes (Table 1). We also found that the frequency-weighted mean recombination rates for each of the autosomes were highly correlated with the direct estimates given in Jensen-Seaman *et al.* (2004) (Pearson correlation = 0.66, $p = 0.002$) and Cox *et al.* (2009) (Pearson correlation = 0.88, $p < 0.0001$), suggesting that our analysis captures real variation in

449 recombination rates at the scale of whole chromosomes in the *M. m. castaneus*
450 genome.
451
452 *Comparison of the* M. m. castaneus *map to maps constructed using inbred lines*
453
454 We compared the intra-chromosomal variation in recombination rates
455 between our *castaneus* map and previously published maps. Figure 2 shows the
456 variation in recombination rates across the largest and smallest autosomes in the
457 mouse genome, chromosomes 1 and 19, respectively. It is clear that the *castaneus*
458 and Cox maps are very similar (see also Figure S2 showing a comparison of all
459 autosomes). Correlation coefficients between the maps are >0.8 for window sizes of
460 8Mbp and above (Figure 3). Although the overall correlation between the *castaneus*
461 and Cox maps is high (Figure 3), there were several regions of the genome that
462 substantially differ, for example in the centre of chromosome 9 (Figure S2). The Cox
463 and *castaneus* maps are more similar to one another than either are to the
464 Brunschwig map (Figure 3), presumably because the Brunschwig map was
465 constructed with a sample of 60 inbred mouse strains. Population structure in the
466 lines or the subspecies from which they were derived would elevate LD, resulting in
467 downwardly-biased chromosome-wide values of ρ. This is also reflected in the N_e
468 values estimated from the frequency-weighted average recombination rates for each
469 chromosome. The estimates of N_e are substantially different between the *castaneus*
470 and Brunschwig maps, i.e. the *castaneus* estimates are consistently ~500x higher
471 (Table 1). The estimates of N_e from the *castaneus* map are in broad agreement with
472 the estimates of N_e based on polymorphism data (Geraldes *et al.* 2008).
473

Correlations between recombination rate and properties of protein coding genes in M. m. castaneus

By examining the correlation between genetic diversity and recombination rate, we determined whether our map captures variation in N_e across the genome. We found that recombination rates at protein coding genes are significantly and positively correlated with levels of neutral genetic diversity (Table 2), at all sites regardless of base context and at non-CpG-prone sites only (Table 2). Divergence from the rat at 4-fold sites was also significantly and positively correlated with recombination rate when analyzing all sites. However, for non-CpG-prone sites we found a small negative correlation (Table 2). There was also a significant and positive relationship between recombination rate and a gene's GC content (τ = 0.125, $p < 2.2\text{x}10^{-16}$). The correlation between recombination rate and neutral diversity divided by divergence from the rat was both positive and significant, regardless of base context (Table 2; Figure S3). This indicates that natural selection may have a role in reducing diversity via hitchhiking and/or background selection.

Discussion

By constructing fine-scale maps of the recombination rate for the autosomes of *M. m. castaneus,* we have shown that there is a high degree of similarity between the recombination landscape for wild-caught mice and their laboratory counterparts. Our map captures variation in the recombination rate, similar to that observed in a more traditional linkage map, at the level of both whole chromosomes and genomic windows of varying size.

Recombination landscapes inferred using coalescent approaches, as in this study, reflect ancestral variation in recombination rates. We show that this ancestral variation is highly correlated with contemporaneous recombination rates in inbred mice of a different subspecies, suggesting that the broad-scale variation in recombination rate has not evolved dramatically since the subspecies diverged around 500,000 years ago (Geraldes *et al.* 2008). At a finer scale, however, Smagulova *et al.* (2016) showed that there is considerable variation in the locations of recombination hotspots between the *M. musculus* subspecies. Their findings, taken together with ours, parallel results in hominids and the great-apes, which suggest that, although the locations of recombination hotspots are strongly diverged between species, broad-scale patterns of recombination rate are relatively conserved (Lesecque *et al.* 2014; Stevison *et al.* 2015). However, there do seem to be multiple regions of the genome that distinguish *M. m. castaneus* and *M. m. domesticus*. For example, we observe peaks in recombination rate for *M. m. castaneus* on chromosomes 4, 5, 14 and 15 that are not present in the Cox map (Figure S2). These results are seemingly consistent with those of Dumont *et al.* (2011), who found that there are significant differences in genetic length between *M. m. castaneus* and *M. m. musculus* (when crossed to *M. m. domesticus*) in multiple regions of the genome (though a large proportion of the differences they detected were on the X-chromosome, which was not analyzed in our study). Performing a comparative analysis of recombination rates in the different subspecies of house mice, as well as sister species, using LD-based methods would help elucidate the time-scale of recombination rate evolution in wild mice.

The *castaneus* map constructed in this study appears to be more similar to the Cox map than the Brunschwig map (Figure 3). There are number of potential reasons for this. Firstly, we used a much larger number of markers to resolve recombination rates than Brunschwig *et al.* (2012), giving us more power to capture variation in the recombination rate. Secondly, it seems probable that population structure within and between the inbred and wild-derived lines studied by Brunschwig *et al.* (2012) could have resulted in biased estimates of the recombination rate. By dividing the mean estimated ρ/bp values (inferred using LDhelmet) for each chromosome by the corresponding recombination rate estimated from crosses (Cox *et al.* 2009), we showed that N_e estimates from the Brunschwig map are much lower than estimates based on our map (Table 1). This is consistent with the presence of elevated LD between the SNPs in the inbred lines analyzed by Brunschwig *et al.* (2012). It should be noted, however, that the estimates of N_e will be biased, as $\theta = 4N_e\mu$ is a parameter in both LDhat and LDhelmet. In spite of this potential bias, the differences in N_e estimated from the Brunschwig and *castaneus* maps shown in Table 1 are striking, given that the ancestral effective population sizes of *M. m. domesticus* and *M. m. castaneus* are expected to be ~150,000 and ~350,000, respectively (Geraldes *et al.* 2008). The Brunschwig map does, however, capture true variation in recombination rates, because their map is also highly correlated with the Cox map (Pearson correlation >0.6) for all genomic windows wider than 8Mbp (Figure 3). Indeed, Brunschwig *et al.* (2012) showed by simulation that hotspots are detectable by analysis of inbred lines and validated their inferred hotspots against the locations of those observed in crosses among classical strains of *M. m. domesticus* (Smagulova *et al.* 2011). This suggests, that while estimates of the recombination rate in the Brunschwig *et al.* (2012) map may have been

549 downwardly biased by population structure, variation in the rate and locations of
550 hotspots were still accurately detected in their study.
551
552 We obtained an estimate of the switch error rate, taking advantage of the
553 hemizygous sex chromosomes of males present in our sample. This allowed us to
554 assess the extent by which switch errors affected our ability to infer recombination
555 rates in *M. m. castaneus*. It should be noted, however, that our inferred switch error
556 rate may not fully represent that of the autosomes. This is because multiple factors
557 influence the ability to phase variants using ShapeIt2 (i.e. LD, SNP density, sample
558 size, depth of coverage and read length) and some of these factors differ between
559 the X-chromosome and the autosomes. Firstly, as the sex-averaged recombination
560 rate for the X-chromosome is expected to be 3/4 that of the autosomes, it likely has
561 elevated LD, and thus there will be higher power to infer phase. In contrast, the level
562 of X-linked nucleotide diversity in *M. m. castaneus* is approximately one half that of
563 the autosomes (Kousathanas *et al.* 2014), and thus there would be a higher
564 probability of phase informative reads on the autosomes. While it is difficult to assess
565 whether the switch error rates we estimated from the X-chromosome analysis will be
566 the same as on the autosomes, the analysis allowed us to explore the effects of
567 different SNP filters on the error rate.
568
569 By simulating the effect of switch errors on estimates of the recombination
570 rate, we inferred the range over which ρ/bp is accurately estimated in our data.
571 Switch errors appear identical to legitimate crossing-over events and, if they are
572 randomly distributed along chromosomes, a specific rate of error will resemble a
573 constant rate of crossing over. The rate of switch error will then determine a

574 detection threshold below which recombination cannot be accurately inferred. We
575 introduced switch errors at random into the simulation data and estimates of ρ/bp
576 obtained from these datasets reflect this detection threshold; below $2x10^{-3}$ ρ/bp, we
577 found that LDhelmet consistently overestimates the recombination rate in the
578 presence of switch errors (Figure 1; Figure S1). This highlights a possible source of
579 bias affecting LD-based recombination mapping studies using inferred haplotypes. In
580 a recent study, Singhal *et al.* (2015) showed that the power to detect recombination
581 hotspots is reduced when the recombination rate in the regions surrounding a
582 hotspot is low. Though we did not attempt to locate recombination hotspots in this
583 study, our findings and those of Singhal *et al.* (2015) both suggest that error in phase
584 inference needs to be carefully considered before attempting to estimate
585 recombination rates and/or recombination hotspots using LD-based approaches.
586
587 Consistent with studies in a variety of organisms, we found a positive
588 correlation between genetic diversity at putatively neutral sites and the rate of
589 recombination. Both unscaled nucleotide diversity and diversity divided by
590 divergence between mouse and rat, a proxy for the mutation rate, are positively
591 correlated with recombination (Table 2). Cai *et al.* (2009) found evidence suggesting
592 that recombination may be mutagenic, though insufficient to account for the
593 correlations they observed between recombination and diversity. The Kendall
594 correlation between π/d_{rat} and recombination rate of 0.20 for all 4-fold sites, a value
595 that is similar in magnitude to the corresponding value of 0.09 reported by Cai *et al.*
596 (2009) in humans. The correlations we report may be downwardly biased, however,
597 because switch errors may result in inflated recombination rates inferred for regions
598 of the genome where the true recombination rate is low (see above). Genes that

599 have recombination rates lower than the detection limit set by the switch error rate
600 may be reported as having inflated ρ/bp (Figure 1; Figure S1), and this would have
601 the effect of reducing correlation statistics. It is difficult to assess the extent of this
602 bias, however, and in any case the correlations we observed between diversity and
603 recombination suggest that our recombination map does indeed capture real
604 variation in N_e across the genome. This indicates that a recombination mediated
605 process influences levels of genetic diversity. Previously, Halligan *et al.* (2013)
606 showed that there are troughs in nucleotide diversity surrounding protein coding
607 exons in *M. m. castaneus*, characteristic of natural selection acting within exons
608 reducing diversity at linked sites. Their results and ours suggest pervasive natural
609 selection in the genome of *M. m. castaneus*.
610
611 In conclusion, we find that sex-averaged estimates of the ancestral
612 recombination landscape for *M. m. castaneus* are highly correlated with
613 contemporary estimates of the recombination rate estimated from crosses of *M. m.*
614 *domesticus* (Cox *et al.* 2009). It has been demonstrated previously that the turnover
615 of hotspots has led to rapid evolution of fine-scale rates of recombination in the *M.*
616 *musculus* subspecies complex (Smagulova *et al.* 2016). On a broad scale, however,
617 our results suggest that the recombination landscape is very strongly conserved
618 between the subspecies. In addition, our estimate of the switch-error rate implies that
619 phasing errors leads to upwardly biased estimates of the recombination rate when
620 the true recombination rate is low. This is a source of bias that should be assessed
621 in future studies. Finally, we showed that the variation in recombination rate is
622 positively correlated with genetic diversity, suggesting that natural selection reduces

623 diversity at linked sites across the *M. m. castaneus* genome, consistent with the
624 findings of Halligan et al (2013).
625
626 To further our understanding of the evolution of the rate of recombination in
627 the house mouse we need to directly compare subspecies. The comparison of our
628 results and previously published maps indicates that there is broad-scale agreement
629 in recombination rates between *M. m. castaneus* and *M. m. domesticus*. In this
630 study, we have assumed that inbred lines derived from *M. m. domesticus* reflect
631 natural variation in recombination rates in that sub-species, though this is not
632 necessarily the case. Population samples like the one studied here could be used to
633 more clearly elucidate the recombination rate maps specific to the different
634 subspecies. A broad survey of this kind would most efficiently be generated using
635 LD-based approaches.
636
637 **Acknowledgements**
638
639 We are grateful to Bettina Harr, Dan Halligan, Ben Jackson and Rory Craig for
640 discussions and helpful comments on the manuscript. Tom Booker is supported by a
641 BBSRC EASTBIO studentship. This project has received funding from the European
642 Research Council (ERC) under the European Union's Horizon 2020 research and
643 innovation programme (grant agreement No. 694212). Rob Ness was funded by the
644 BBSRC (BB/L00237X/1).
645
646
647

Literature Cited

Auton, A., and G. McVean, 2007 Recombination rate estimation in the presence of hotspots. Genome Res 17: 1219-1227.

Baines, J. F., and B. Harr, 2007 Reduced x-linked diversity in derived populations of house mice. Genetics 175: 1911-1921.

Baudat, F., J. Buard, C. Grey, A. Fledel-Alon, C. Ober *et al.*, 2010 Prdm9 is a major determinant of meiotic recombination hotspots in humans and mice. Science 327: 836-840.

Baudat, F., Y. Imai and B. de Massy, 2013 Meiotic recombination in mammals: Localization and regulation. Nat Rev Genet 14: 794-806.

Brick, K., F. Smagulova, P. Khil, R. D. Camerini-Otero and G. V. Petukhova, 2012 Genetic recombination is directed away from functional genomic elements in mice. Nature 485: 642-645.

Brunschwig, H., L. Liat, E. Ben-David, R. W. Williams, B. Yakir *et al.*, 2012 Fine-scale maps of recombination rates and hotspots in the mouse genome. Genetics 191: 757-764.

Cai, J. J., J. M. Macpherson, G. Sella and D. A. Petrov, 2009 Pervasive hitchhiking at coding and regulatory sites in humans. PLoS Genet 5: e1000336.

Chan, A. H., P. A. Jenkins and Y. S. Song, 2012 Genome-wide fine-scale recombination rate variation in drosophila melanogaster. PLoS Genet 8: e1003090.

Cox, A., C. L. Ackert-Bicknell, B. L. Dumont, Y. Ding, J. T. Bell *et al.*, 2009 A new standard genetic map for the laboratory mouse. Genetics 182: 1335-1344.

Cutter, A. D., and B. A. Payseur, 2013 Genomic signatures of selection at linked sites: Unifying the disparity among species. Nat Rev Genet 14: 262-274.

673 Davies, B., E. Hatton, N. Altemose, J. G. Hussin, F. Pratto *et al.*, 2016 Re-
674 engineering the zinc fingers of prdm9 reverses hybrid sterility in mice. Nature
675 530**:** 171-176.
676 Delaneau, O., B. Howie, A. J. Cox, J. F. Zagury and J. Marchini, 2013 Haplotype
677 estimation using sequencing reads. Am J Hum Genet 93**:** 687-696.
678 Dumont, B. L., M. A. White, B. Steffy, T. Wiltshire and B. A. Payseur, 2011 Extensive
679 recombination rate variation in the house mouse species complex inferred
680 from genetic linkage maps. Genome Res 21**:** 114-125.
681 Geraldes, A., P. Basset, B. Gibson, K. L. Smith, B. Harr *et al.*, 2008 Inferring the
682 history of speciation in house mice from autosomal, x-linked, y-linked and
683 mitochondrial genes. Mol Ecol 17**:** 5349-5363.
684 Grey, C., P. Barthes, G. Chauveau-Le Friec, F. Langa, F. Baudat *et al.*, 2011 Mouse
685 prdm9 DNA-binding specificity determines sites of histone h3 lysine 4
686 trimethylation for initiation of meiotic recombination. PLoS Biol 9**:** e1001176.
687 Halligan, D. L., A. Kousathanas, R. W. Ness, B. Harr, L. Eory *et al.*, 2013
688 Contributions of protein-coding and regulatory change to adaptive molecular
689 evolution in murid rodents. PLoS Genet 9**:** e1003995.
690 Halligan, D. L., F. Oliver, A. Eyre-Walker, B. Harr and P. D. Keightley, 2010
691 Evidence for pervasive adaptive protein evolution in wild mice. PLoS Genet 6**:**
692 e1000825.
693 Halligan, D. L., F. Oliver, J. Guthrie, K. C. Stemshorn, B. Harr *et al.*, 2011 Positive
694 and negative selection in murine ultraconserved noncoding elements. Mol Biol
695 Evol 28**:** 2651-2660.
696 Hudson, R. R., 2001 Two-locus sampling distributions and their applications.
697 Genetics 159**:** 12.

698 Jensen-Seaman, M. I., T. S. Furey, B. A. Payseur, Y. Lu, K. M. Roskin *et al.*, 2004
699 Comparative recombination rates in the rat, mouse and human genomes.
700 Genome Res 14**:** 528-538.
701 Johnston, S. E., C. Berenos, J. Slate and J. M. Pemberton, 2016 Conserved genetic
702 architecture underlying individual recombination rate variation in a wild
703 population of soay sheep (ovis aries). Genetics 203**:** 583-598.
704 Kousathanas, A., D. L. Halligan and P. D. Keightley, 2014 Faster-x adaptive protein
705 evolution in house mice. Genetics 196**:** 1131-1143.
706 Lesecque, Y., S. Glemin, N. Lartillot, D. Mouchiroud and L. Duret, 2014 The red
707 queen model of recombination hotspots evolution in the light of archaic and
708 modern human genomes. PLoS Genet 10**:** e1004790.
709 Li, H., and R. Durbin, 2009 Fast and accurate short read alignment with burrows-
710 wheeler transform. Bioinformatics 25**:** 1754-1760.
711 Li, H., B. Handsaker, A. Wysoker, T. Fennell, J. Ruan *et al.*, 2009 The sequence
712 alignment/map format and samtools. Bioinformatics 25**:** 2078-2079.
713 Liu, E. Y., A. P. Morgan, E. J. Chesler, W. Wang, G. A. Churchill *et al.*, 2014 High-
714 resolution sex-specific linkage maps of the mouse reveal polarized distribution
715 of crossovers in male germline. Genetics 197**:** 91-106.
716 McVean, G., P. Awadalla and P. Fearnhead, 2002 A coalescent-based method for
717 detecting and estimating recombination from gene sequences. Genetics 160**:**
718 1231-1241.
719 McVean, G., S. R. Myers, S. Hunt, P. Deloukas, D. R. Bentley *et al.*, 2004 The fine-
720 scale structure of recombination rate variation in the human genome. Science
721 304.

722 Messer, P. W., 2013 Slim: Simulating evolution with selection and linkage. Genetics
723 194**:** 1037-1039.
724 Myers, S. R., R. Bowden, A. Tumian, R. E. Bontrop, C. Freeman *et al.*, 2010 Drive
725 against hotspot motifs in primates implicates the prdm9 gene in meiotic
726 recombination. Science 327.
727 Paigen, K., and P. Petkov, 2010 Mammalian recombination hot spots: Properties,
728 control and evolution. Nat Rev Genet 11**:** 221-233.
729 Paigen, K., J. P. Szatkiewicz, K. Sawyer, N. Leahy, E. D. Parvanov *et al.*, 2008 The
730 recombinational anatomy of a mouse chromosome. PLoS Genet 4**:**
731 e1000119.
732 RCoreTeam, 2016 R: A language and environment for statistical computing., pp. R
733 Foundation for Statistical Computing, Vienna Austria.
734 Schwartz, J. J., D. J. Roach, J. H. Thomas and J. Shendure, 2014 Primate evolution
735 of the recombination regulator prdm9. Nat Commun 5**:** 4370.
736 Singhal, S., E. Leffler, K. Sannareddy, I. Turner, O. Venn *et al.*, 2015 Stable
737 recombination hotspots in birds. Science 350**:** 6.
738 Smagulova, F., K. Brick, P. Yongmei, R. D. Camerini-Otero and G. V. Petukhova,
739 2016 The evolutionary turnover of recombiantion hotspots contributes to
740 speciation in mice. Genes & Development 30**:** 277-280.
741 Smagulova, F., I. V. Gregoretti, K. Brick, P. Khil, R. D. Camerini-Otero *et al.*, 2011
742 Genome-wide analysis reveals novel molecular features of mouse
743 recombination hotspots. Nature 472**:** 375-378.
744 Smukowski, C. S., and M. A. Noor, 2011 Recombination rate variation in closely
745 related species. Heredity (Edinb) 107**:** 496-508.

Smukowski Heil, C. S., C. Ellison, M. Dubin and M. A. Noor, 2015 Recombining without hotspots: A comprehensive evolutionary portrait of recombination in two closely related species of drosophila. Genome Biol Evol 7**:** 2829-2842.

Stevison, L. S., K. B. Hoehn and M. A. Noor, 2011 Effects of inversions on within- and between-species recombination and divergence. Genome Biol Evol 3**:** 830-841.

Stevison, L. S., A. E. Woerner, J. M. Kidd, J. L. Kelley, K. R. Veeramah *et al.*, 2015 The time scale of recombination rate evolution in great apes. Mol Biol Evol.

Wang, R. J., M. M. Gray, M. D. Parmenter, K. W. Broman and B. A. Payseur, 2017 Recombination rate variation in mice from an isolated island. Mol Ecol 26**:** 457-470.

Winckler, W., S. R. Myers, D. J. Richter, R. C. Onofrio, G. J. McDonald *et al.*, 2005 Comparison of fine-scale recombination rates in humans and chimpanzees. Science 308.

Yang, H., J. R. Wang, J. P. Didion, R. J. Buus, T. A. Bell *et al.*, 2011 Subspecific origin and haplotype diversity in the laboratory mouse. Nat Genet 43**:** 648-655.

771 **Figures and Tables**

772

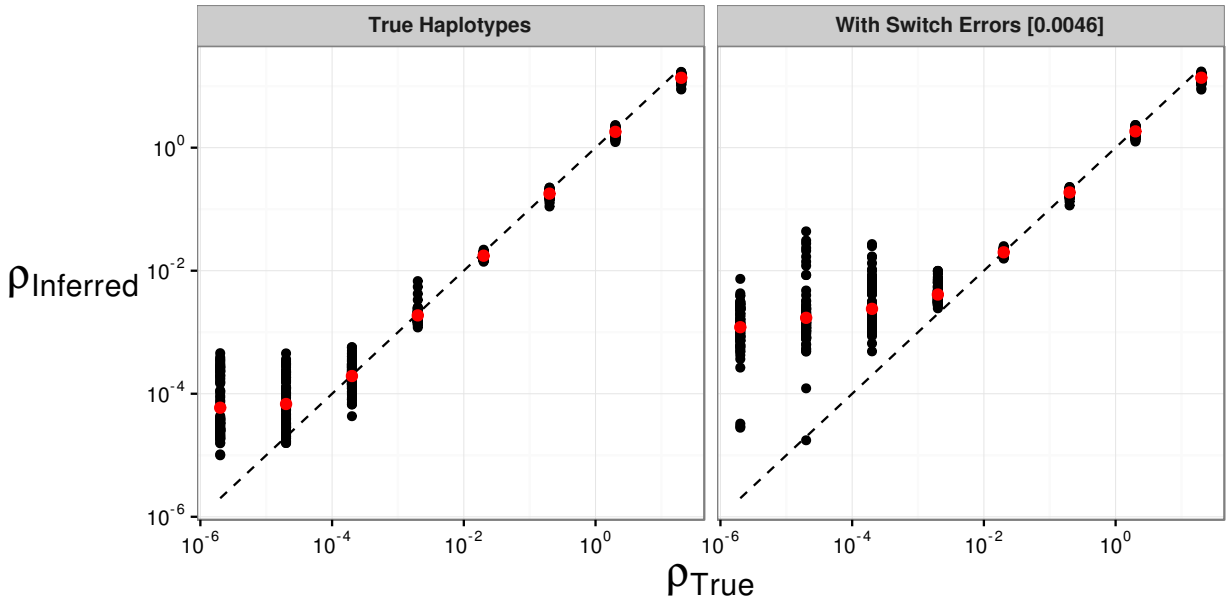

773

774 **Figure 1** The effect of switch errors on the mean recombination rate inferred using LDhelmet
775 with a block penalty of 100. Each black point represents results for a window of 4,000 SNPs,
776 with 200 SNPs overlapping between adjacent windows, using sequences simulated in SLiM
777 for a constant value of ρ/bp. Red points are mean values. Switch errors were randomly
778 incorporated at heterozygous SNPs with probability 0.0046. The dotted line shows the value
779 for inferred=true.

780

781

782

783

784

785

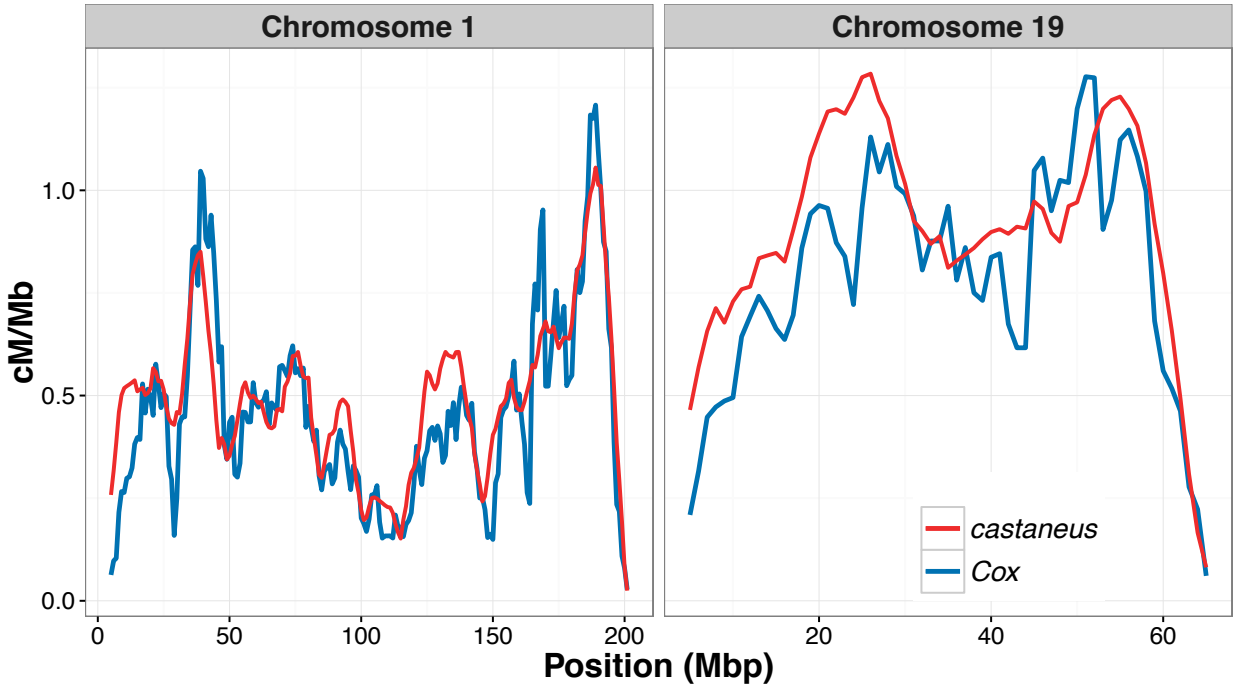

Figure 2 Comparison of the sex-averaged recombination rate inferred for chromosomes 1 and 19 of *M. musculus castaneus* using LDhelmet in red and those estimated from the pedigree-based study of Cox *et al.* (2009) in blue. Recombination rates in units of cM/Mb for the *castaneus* map were obtained by setting the total genetic lengths for each chromosome to the corresponding lengths from Cox *et al.* (2009).

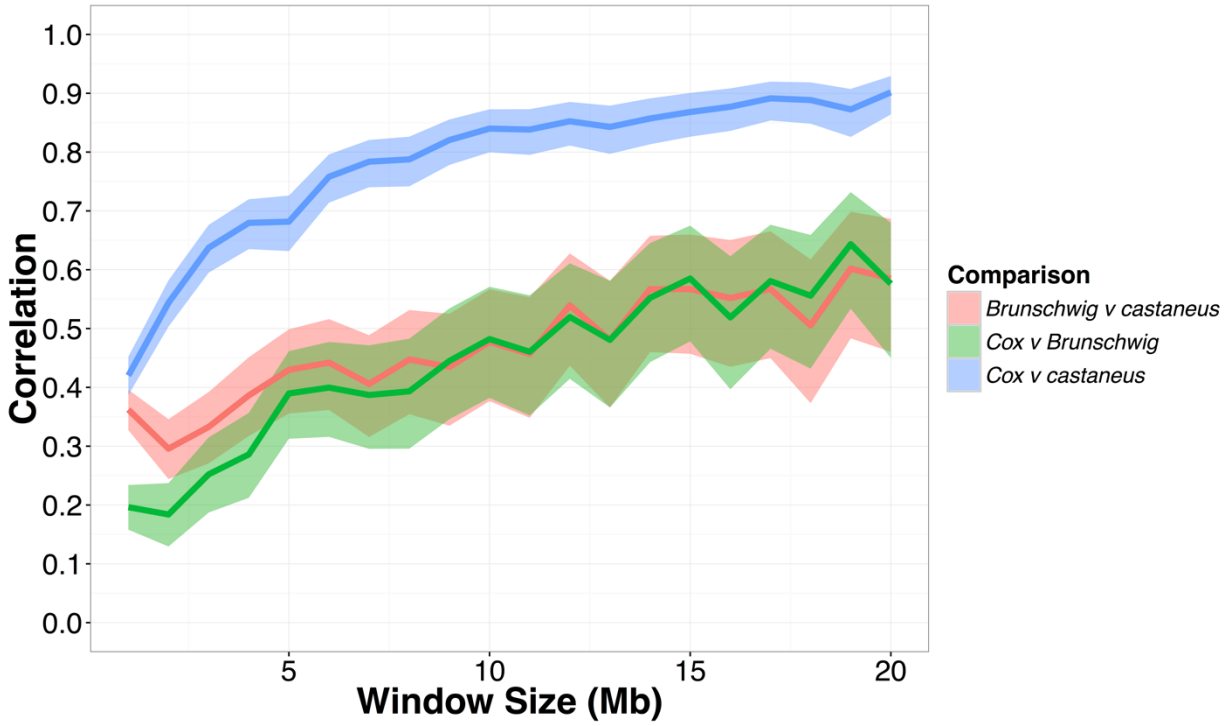

799

800 **Figure 3** Pearson correlation coefficients between the recombination map inferred for *M. m.*

801 *castaneus,* the Brunschwig *et al.* (2012) map and the Cox *et al.* (2009) map. Correlations

802 were calculated in non-overlapping windows of varying size across all autosomes.

803 Confidence intervals (95%) are indicated by shading around each line.

804

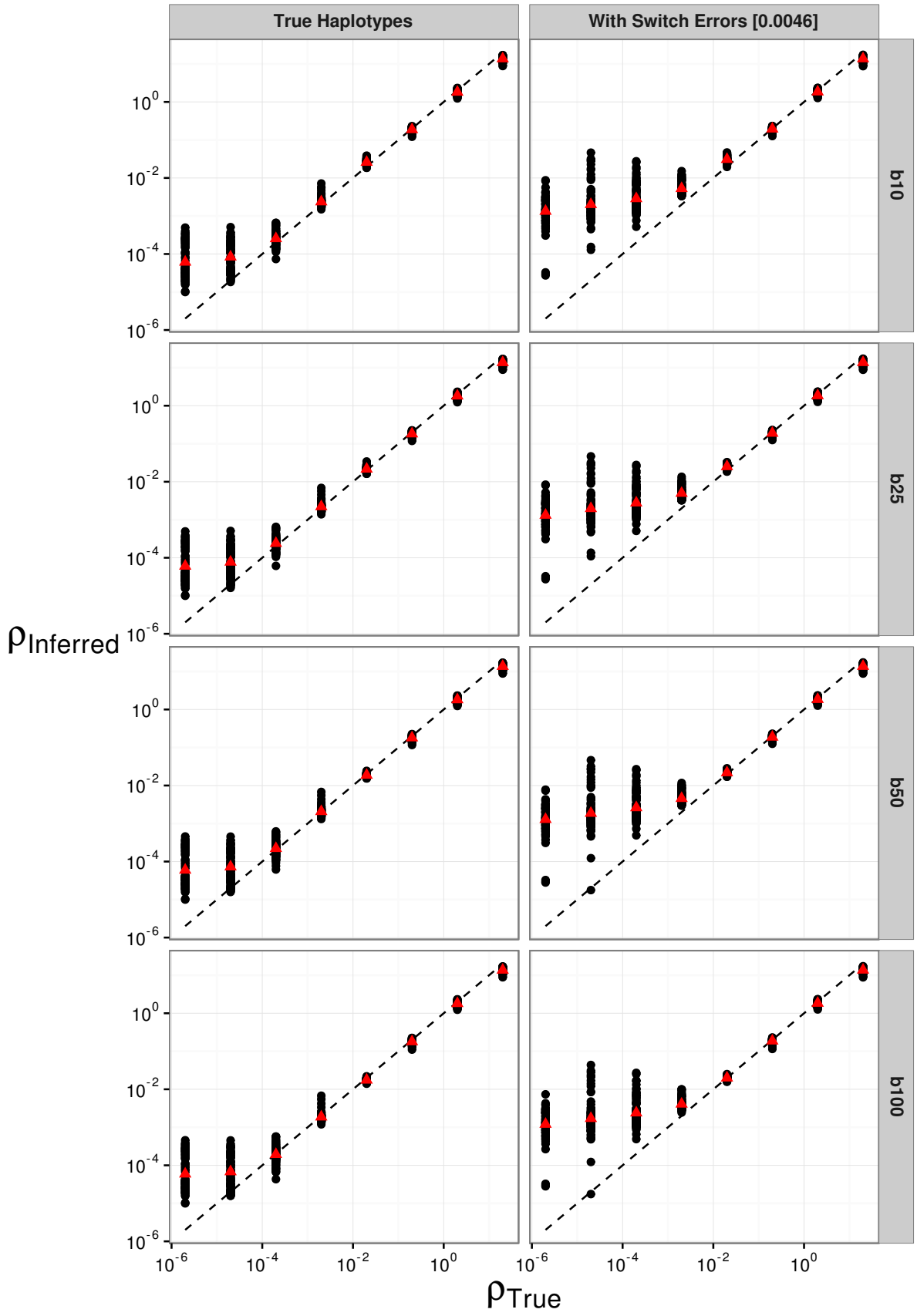

805

806 **Figure S1** The effect of switch errors and block penalty on the mean recombination rate
807 inferred using LDhelmet. Block penalties (b) of 10, 25, 50 and 100 were used, shown in the
808 vertically ordered facets from top to bottom.
809
810
811
812
813
814
815

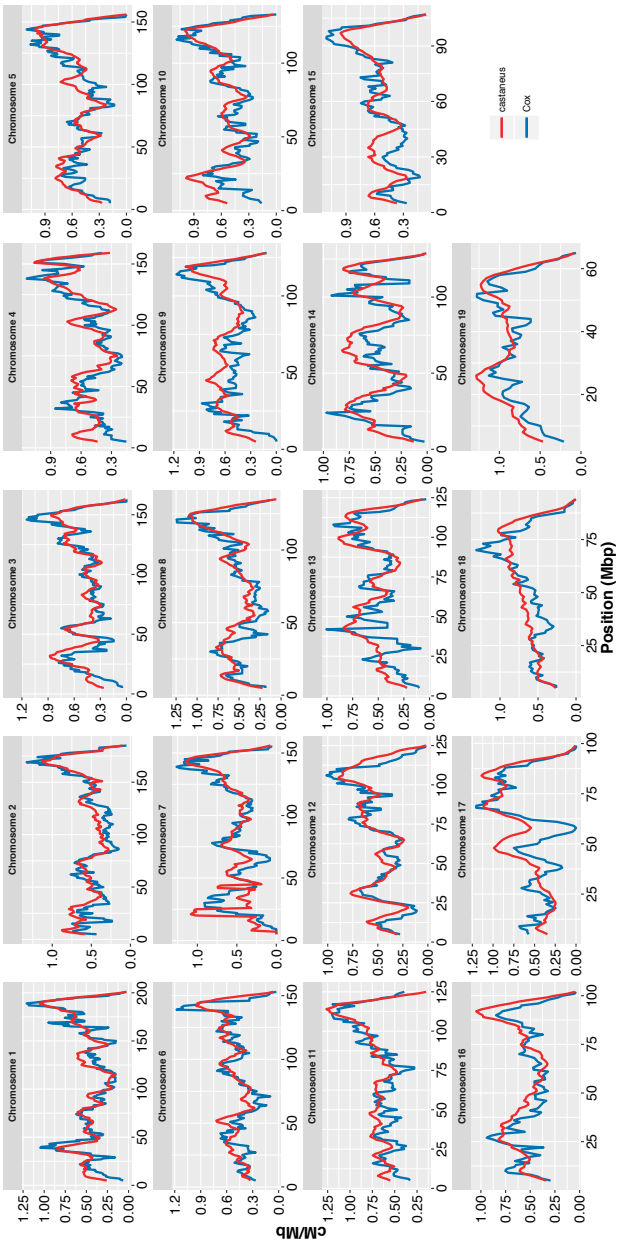

Figure S2 Comparison of recombination rates inferred for *M. m. castaneus* using LDhelmet and recombination rates reported by Cox et al (2009). Recombination rates in units of ρ/bp for the *castaneus* map were converted to cM/Mb by scaling using the genetic length of the corresponding chromosome in the Cox map.

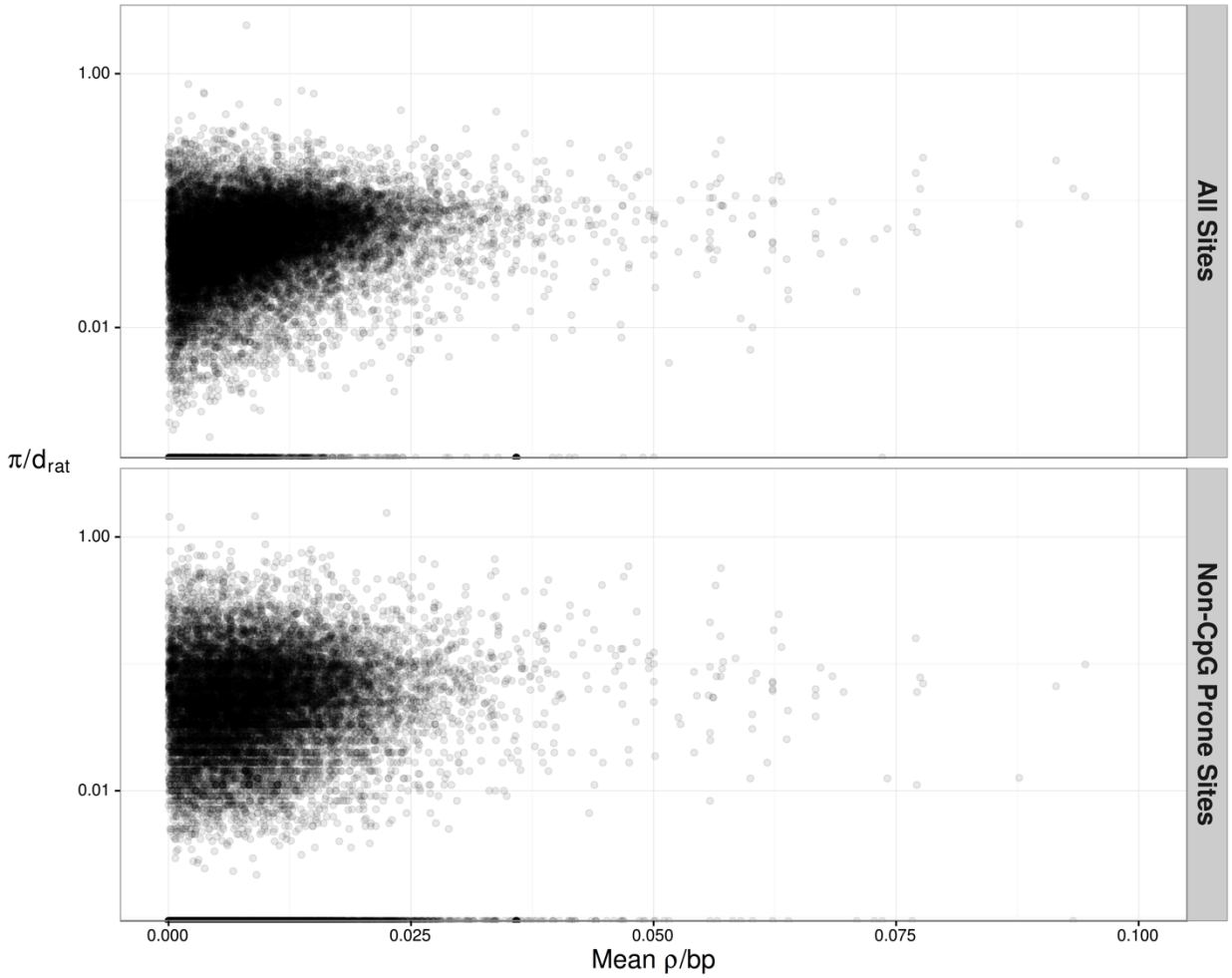

821

822

823 **Figure S3** Nucleotide diversity divided by divergence from rat (π/d_{rat}) at 4-fold degenerate
824 synonymous sites plotted against the frequency weighted mean recombination rates (ρ/bp)
825 for protein coding genes in *M. m. castaneus*. Correlation statistics are shown in the main
826 text. For the purposes of visualization, the range of ρ/bp is restricted from 0 to 0.1. There are
827 19 genes that have mean ρ/bp >0.1, however.

828

829

830

831

832

833

834 **Table 1**

835 Summary of sex-averaged recombination rates estimated for the *M. m castaneus*
836 autosomes compared with the rates from Brunschwig *et al.* (2012) and Cox *et al.* (2009).
837 Rates for the *castaneus* and Brunschwig maps are presented in terms of $4N_e r$/bp. Estimates
838 of N_e were obtained by assuming the recombination rates from Cox *et al.* (2009).

839

Chromosome	Cox cM/Mb	*castaneus*		Brunschwig	
		Freq. Weighted Mean	N_e Estimate	Freq. Weighted Mean	N_e Estimate
1	0.50	0.0079	395,000	0.000015	745
2	0.57	0.0088	386,000	0.000015	653
3	0.52	0.0083	400,000	0.000014	693
4	0.56	0.0091	408,000	0.000020	889
5	0.59	0.0090	382,000	0.000015	646
6	0.53	0.0089	421,000	0.000015	728
7	0.58	0.0100	429,000	0.000019	801
8	0.58	0.0094	404,000	0.000014	610
9	0.61	0.0096	394,000	0.000018	749
10	0.61	0.0096	392,000	0.000023	928
11	0.70	0.0102	365,000	0.000019	689
12	0.53	0.0089	420,000	0.000019	897
13	0.56	0.0095	426,000	0.000014	629
14	0.53	0.0084	395,000	0.000013	632
15	0.56	0.0083	371,000	0.000024	1,080
16	0.59	0.0091	386,000	0.000017	721
17	0.65	0.0087	335,000	0.000052	2,020
18	0.66	0.0098	371,000	0.000021	785
19	0.94	0.0122	323,000	0.000026	681
Mean		0.0092		0.000020	

Table 2

Correlation coefficients between recombination rate and pairwise nucleotide diversity and divergence from the rat at 4-fold degenerate sites for protein coding genes. Non-parametric Kendall correlations were calculated for non-CpG prone sites and for all sites, regardless of base context. All coefficients shown are highly significant ($p < 10^{-10}$).

	Non-CpG	All Sites
Nucleotide diversity (π)	0.09	0.20
Divergence to rat (d_{rat})	-0.04	0.06
Corrected diversity (π/d_{rat})	0.10	0.18

Table S1

The effect of different filters on the frequency of switch errors in the haplotypes inferred based on the three pseudo-females. The values in the switch errors column are the raw numbers of switch errors and the total number of heterozygous SNPs on the X-chromsome. Variants with Quality (QUAL) <30 were excluded for all filter sets.

Filter Set	HWE*	Min DP†	Max DP	Min GQ‡	Switch Errors			Switch Error Rate
					H40	*H46*	*H62*	
1	-	-	-	-	5148 / 409486	4819 / 407422	5020 / 394778	0.0124
2	<0.0002	10	-	15	1690 / 338592	1451 / 334111	1452 / 324199	0.0046
3	<0.0002	10	100	5	2460 / 341744	2066 / 339508	2536 / 328998	0.0070
4	<0.0002	-	-	40	523 / 288471	444 / 286636	550 / 281266	0.0018

**HWE refers to the p-value for the Samtools Hardy-Weinberg equilibrium test below which variants were excluded.*

†Depth of coverage per individual.

‡Per individual genotype quality scores.

883 **Table S2**

884 The normalized mutation rate matrix and stationary distribution of base frequencies

885 estimated with two out-groups, *M. famulus* and *R. norvegicus*, using the method described

886 by Chan *et al.* (2012).

	A	C	G	T
A	0.48	0.09	0.32	0.11
C	0.19	0.00	0.12	0.69
G	0.69	0.12	0.00	0.19
T	0.11	0.32	0.08	0.48
Stationary Distribution	0.34	0.16	0.16	0.34

887